Turk J Elec Eng & Comp Sci, Vol.18, No.3, 2010, © TÜBİTAK
doi:10.3906/elk-0912-12

Antenna systems with beam forming and beam steering capabilities for HF skywave radars

Çağatay ULUIŞIK
Electronics and Communications Engineering Department, Doğuş University
Acıbadem, 34722, İstanbul-TURKEY
e-mail: culuisik@dogus.edu.tr

Abstract

Radiation characteristics of linearly phased, periodic, planar dipole arrays, which can be used as transmitting/receiving antenna systems for HF skywave radars, are investigated. Rectangular, triangular and trapezoidal arrays are proposed in obtaining different beam shapes in the desired directions. Beam steering is achieved by adjusting the inter-element phase increments coherently. The effects of vertical array-tilt with a desired take-off angle (TOA) α are presented by a number of radiation pattern examples. The ground effect is investigated using the image theory by assuming the Earth's surface as perfectly electric conductor (PEC). Radiated fields are obtained using Floquet wave representations plus the synthetic aperture approach. Validation is done against element-by-element summation representations.

Key Words: *HF radars, HF communication, Skywaves, ionospheric reflections, Earth- ionosphere waveguide, planar arrays, phased array antennas, beam forming, beam steering.*

1. Introduction

Long range, over-the-horizon radar and communication systems use high frequencies (HF) and Earth-Ionosphere waveguides [1-3]. Skywaves refer to the propagation of electromagnetic (EM) waves reflected back and forth between the Earth's surface and the Ionosphere. Skywaves propagate between the Earth and Ionosphere, which occupies a region above the troposphere, about 50 to 250 miles above the Earth, where neutral air is ionized by solar photons and cosmic rays. Groundwave propagation, skywave propagation and the effects of the Ionosphere are illustrated in Figure 1.

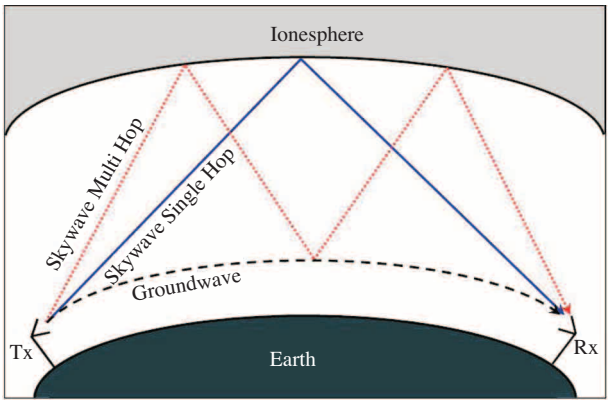

Figure 1. Groundwave-skywave propagation and the effects of the ionosphere.

Skywaves can propagate many thousands of kilometers via multiple reflections called hoping. While HF groundwave propagation over the sea has been used for distances up to several hundred kilometers, radars operating in the HF band and using skywaves can detect targets at ranges of thousands of kilometers beyond-the-horizon well into diffraction region.

Skywave HF radars and/or communication systems necessitate antenna systems with broad transmit and narrow (angle sensitive) receive capabilities [4]. HF receive antenna systems also require high beam forming and beam steering capabilities. Resonant wire antennas of dipoles and/or monopoles are widely used in HF antenna systems. Since the wavelengths are very long in the HF band (100m to 10m), so are the sizes of the HF antennas. Therefore HF radars do not physically rotate antennas to change the direction of the beam. Instead the beam steering is achieved by adjusting the amplitude and the phase of the signals from each element. Such arrays, where relative phases of the elements are changed in such a way that the main beam in the radiation pattern shows a desired direction are called phased arrays.

A large number of different array configurations are investigated in the literature [4-12]. Periodic, linear and planar dipole arrays have been extensively investigated by the late L. B. Felsen and his collaborators [8, 9]. This paper aims to investigate periodic, linearly phased, planar, dipole arrays confined in different shaped regions such as rectangular, triangular or trapezoidal areas.

The HF radars are mostly used for maritime surveillance where the skywave propagates over the water. Due to the high conductivity of the water, the Earth's surface can be supposed as PEC (Perfect Electric Conductor) where the conductivity is infinite ($\sigma = \infty$) and the ground effect can be taken into account by using the image theory. Therefore, for the investigated arrays, the ground is replaced by a mirror array of the original array with respect to the Earth's surface and the total field is obtained via superposition of the fields radiated by the original array and the mirror array. So the effect of the ground is also investigated.

2. Statement of the Problem and Formulation

2.1. Element-by-Element Summation Representation

The geometry of the rectangular periodic array of $N_x \times N_z$ infinitesimal z-directed dipoles with unit current amplitude is shown in Figure 2(a). The interelement spacing is d_x and d_z in the x and z directions. The dipoles

are linearly phased with $k\eta_x d_x$ and $k\eta_z d_z$, which denote the interelement phase increments along the x and z coordinates, respectively.

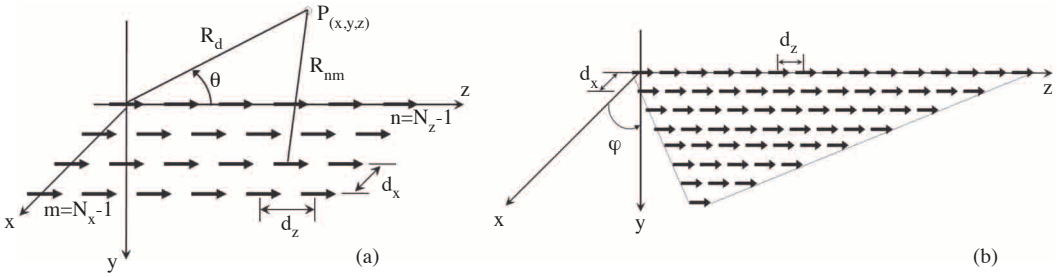

Figure 2. Geometry of the **(a)** rectangular **(b)** triangular array of electric current dipoles.

The radiated field is determined by the z-component of the magnetic vector potential $A_z(\omega)$ and under the assumed $\exp(j\omega t)$ time-dependence $A_z(\omega)$ can be expressed as

$$A_z(\omega) = \sum_{m=0}^{N_x-1} \sum_{n=0}^{N_z-1} \frac{e^{-jkR_{nm}}}{4\pi R_{nm}} e^{-j(k\eta_x m d_x + k\eta_z n d_z)} \tag{1a}$$

$$R_{nm} = \sqrt{(x - md_x)^2 + y^2 + (z - nd_z)^2}. \tag{1b}$$

Figure 2(b) shows an array consisting of N_x rows along x direction each with $N_z - 2m$ elements (m=0,1,2, $\ldots, N_x-1$) along z direction, so that the first (m=0) row has N_z and the last (m=N_x-1) row has (N_z-2N_x+2) elements. If $N_z = 2N_x - 1$, the last row has only one element and the array is triangular, otherwise the last row has more than one element and the array becomes trapezoidal. The interelement period is d_x and d_z. along the x and z coordinates and the normalized interelement phasings in the x and z directions are η_x and η_z, respectively. $A_z(\omega)$ radiated by the specified triangular / trapezoidal array can be expressed as

$$A_z(\omega) = \sum_{m=0}^{N_x-1} \sum_{n=m}^{(N_z-1-m)} \frac{e^{-jkR_{nm}}}{4\pi R_{nm}} e^{-j(k\eta_x m d_x + k\eta_z n d_z)}. \tag{2}$$

A short MatLab code for the calculation of vertical radiation patterns of a triangular array by using the element-by-element summation is provided in Table.

2.2. Floquet wave (FW) representation

The calculation of element-by-element summation in (1a) and (2) is numerically inefficient for arrays consisting large number of dipoles. In order to improve numerical efficiency Floquet waves can be used. We will start our Floquet wave analysis with the field radiated by a semi-infinite line array given in [9] and reproduced below:

$$A_z(\omega) = \frac{e^{-jkR_d}}{4\pi\, R_d} + \sum_q A_q^{FW}\, U(\beta_q - \theta) \tag{3a}$$

where

Table. A MatLab script for plotting the vertical radiation pattern of a triangular array.

```
c=3e8; freq=4e6; lamd=c/freq; k=2*pi/lamd;
dx=lamd/4; dz=lamd/4; etax=1; etaz=0;
Nz=15; dN=1; Nx=8; RR=100*lamd; z=0; nn=1;
for theta=.01:.01:2*pi
   x=RR*cos(theta); y=RR*sin(theta); Azz=0;
   for m=0:(Nx-1)
     for n=m*dN:(Nz-1)-m*dN
       Rnm=sqrt((x-m*dx)^2+(y-0.2*lamd)^2+(z-n*dz)^2);
       P1=exp(-j*k*Rnm)/(4*pi*Rnm);
       P2=exp(-j*(k*etax*m*dx+k*etaz*n*dz));
       Azz=Azz+P1*P2;
     end
   end
   Thetar(nn)=theta; Az(nn)=Azz; nn=nn+1;
end
A1=(abs(Az)); A2=A1/max(A1); polar(Thetar,A2)
```

$$A_q^{FW} \approx \frac{e^{-j\,(k_{\rho\,q}\rho + k_{zq} z + \pi/4)}}{2d_z\sqrt{2\pi\, k_{\rho\,q}\rho}}, \quad \beta_q = \cos^{-1}(k_{zq}/k) \quad \rho^2 = x^2 + y^2 \tag{3b}$$

The z-domain wavenumber k_{zq} and the radial wavenumber $k_{\rho\,q}$ are determined by $k_{z\,q} = k\eta_z + 2\pi\, q/d_z$ and $k_{\rho\,q} = \sqrt{k^2 - k_{zq}^2}$. A_q^d in (3a) corresponding to the tip diffracted waves is expressed as

$$A_q^d = \frac{\pm e^{-jkR_d}\sqrt{\pi}\delta_q\, e^{j\delta_q^2}\, e^{j\pi/4} erfc(\pm e^{j\pi/4}\delta_q)}{4\pi\, R_d jkd_z\, [\cos(\beta_q) - \cos(\theta)]}, \quad \delta_q = \sqrt{2kR_d}\sin\left(\frac{\beta_q - \theta}{2}\right). \tag{3c}$$

U(.) is the Heaviside unit function and $erfc(.)$ stands for the complementary error function.

The field radiated by a finite line array consisting of N_z dipoles can be found as a superposition of two semi-infinite line arrays where one of them is shifted distance $N_z d_z$ along the z coordinate and oppositely phased with respect to the other. Using a synthetic aperture approach [11], the field at an observation point radiated by the shifted array can be imagined as the field at a virtual oppositely shifted observation point radiated by the original array and weighted with an appropriate phase shift. The field radiated by a rectangular /triangular array can be expressed as a superposition of the fields radiated by finite line arrays. The synthetic aperture approach can be extended to two dimensions and the fields radiated by the finite line arrays shifted by distance d_x along x with respect to each other can be imagined as the field radiated by the original finite line array at virtual oppositely shifted observation points.

For the following proposed array configurations horizontal and vertical radiation patterns are calculated using Floquet waves and also element-by-element summation representations.

3. Characteristic examples

Characteristic examples and typical results are presented in this section. The first case, illustrated in Figure 3(a), belongs to a periodic line array consisting of N_z=15 infinitesimal z-directed dipoles with unit current amplitude. The interelement spacing is chosen to be $d_z = \lambda/4$. For an HF radar operating at the frequency f=4MHz, the

interelement spacing is $d_z = 18.75$ m. The dipoles are linearly phased with the normalized interelement phasing η_z. However, for this particular example $\eta_z = 0$. Figure 3(b) shows the amplitude of the magnetic scalar potential $A_z(\omega)$ versus θ in the x-z plane at a radial distance $R_d = 100\lambda$ radiated by this line array. This variation of $|A_z(\omega)|$ in the far field can be considered as the horizontal radiation pattern of the array and it can be seen from the figure that the radiation is in the broadside direction. Figure 3(c) shows the variation of $|A_z(\omega)|$ versus φ in the x-y plane at a radial distance $R_d = 100\lambda$ which is the vertical radiation pattern of the line array. Since the ground effect is not taken into account in Figure 3(c), the vertical radiation pattern is isotropic. The effect of a PEC ground is added in Figure 3(d) by obtaining the total field as a superposition of the fields radiated by the original array and by a mirror array of the original array with respect to x-z plane. While the ground effect changes the vertical radiation pattern from being isotropic to a single beam in the y-direction, it does not affect the horizontal radiation pattern. In all radiation patterns in the following examples, throughout this paper, the blue solid curves correspond to element-by-element summation solutions and the red dashed curves correspond to Floquet wave representations.

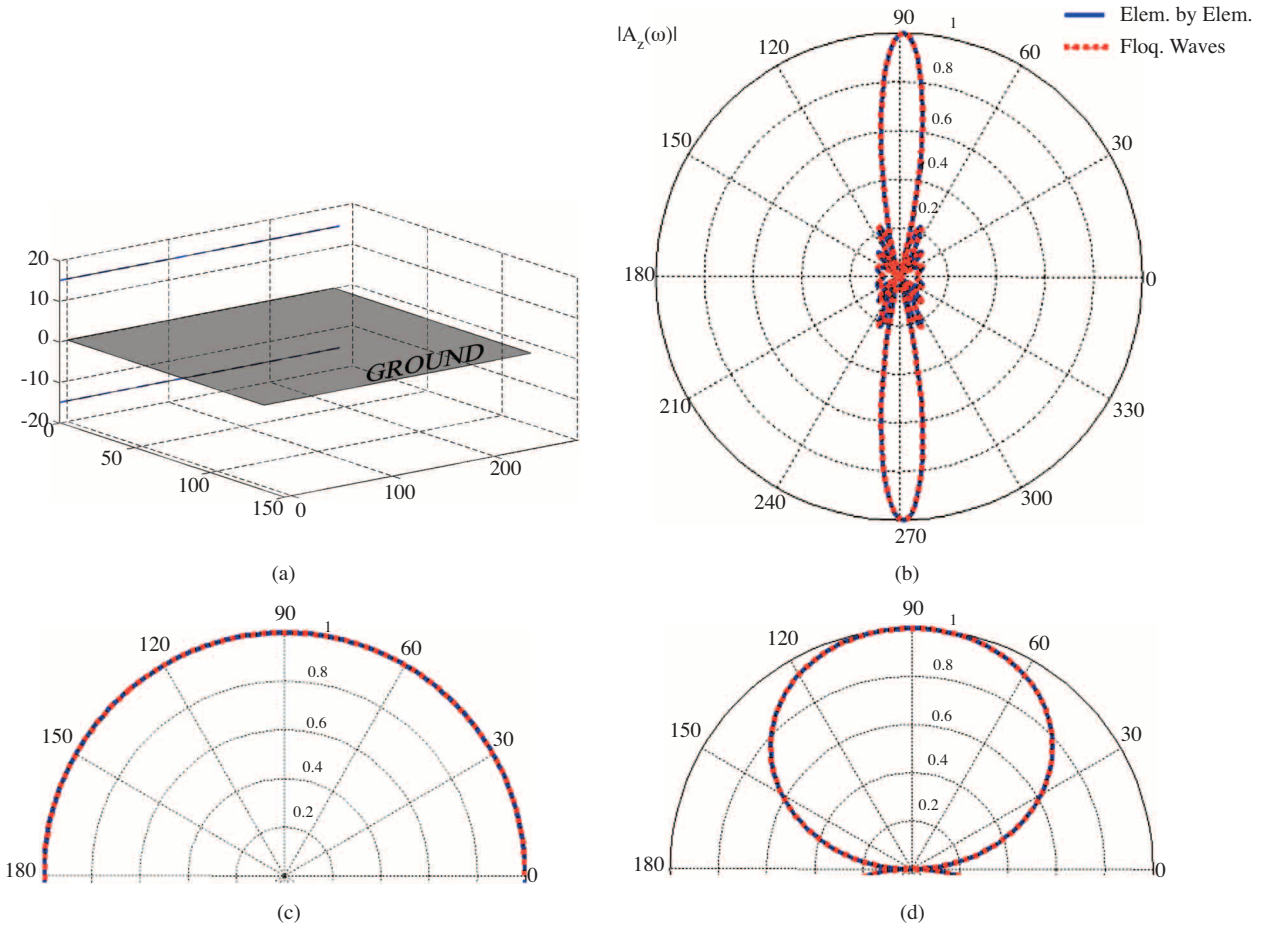

Figure 3. **(a)** Periodic line array of axial electric current dipoles located along the z-axis **(b)** Horizontal radiation pattern **(c)** Vertical radiation pattern without the ground effect **(d)** Vertical radiation pattern with the PEC ground ($N_z = 15$, $d_z = \lambda/4$, $\eta_z = 0$).

A rectangular array consisting of N_z=15 and N_x=8 dipoles in the z and x directions, respectively, is illustrated in Figure 4(a) with its mirror array. The interelement spacings are $d_z = d_x = \lambda/4$ and the interelement phasing along the x coordinate is η_x=1. The horizontal radiation patterns for different interelement phasings η_z are plotted in Figures 4(c - f). The interelement distances d_z, d_x and η_x are so chosen that the array produces a single beam and the beam can be steered to the desired direction by appropriately changing η_z. For η_z=0 the beam is in the broadside direction (θ=90°) as shown in Figure 4(c). For increasing positive η_z values the beam is directed to θ values decreasing from 90° as shown in Figures 4(d), 4(e) and for decreasing negative η_z values the beam is directed to θ values increasing from 90° as shown in Figure 4(f). The vertical radiation pattern is plotted in Figure 4(b) which is independent from η_z.

Figure 5(a) shows a triangular array consisting of 8 rows (m=0, 1, 2, 3, 4, 5, 6, 7) along x-direction each with (15-2m) elements along z-direction, so that the first (m=0) row has 15 and the last (m=7) row has only one element. The interelement distances are $d_z = d_x = \lambda/4$ and the normalized interelement phasings are η_z=0, η_x=1. The array is tilted by a take-off angle α in the φ-direction as shown in the figure. The horizontal radiation pattern, which is not effected by the angle α, is plotted in Figure 5(b). The vertical radiation patterns for α=0°, 15°, 30°, 45°, 60°, 75° are presented in Figures 5(c-h), respectively. It can be easily concluded from the figures that rotating the array by an angle of α, rotates the main beam by 2α. This attribute is analogous to the optical reflection rule, rotating a mirror by an angle α rotates the reflected ray by 2α.

The triangular array in Figure 5(a) consisting of N_z=15-2m (m=0, 1, 2, 3, 4, 5, 6, 7) and N_x=8 dipoles in the z and x directions, respectively, is illustrated in Figure 6(a) with its mirror array corresponding to the PEC ground. The interelement distances are again $d_z = d_x = \lambda/4$ and η_x=1. The horizontal radiation patterns for η_z=0, 0.5, 0.75, -0.75 are shown in Figures 6(b-e), respectively. Similar to the rectangular array in Figure 4(a), the beam steering in the horizontal pattern is achieved by changing η_z coherently. The beam is in the broadside direction (θ=90°) for η_z=0 as shown in Figure 6(b). The beam is directed to θ values less than 90° for positive η_z values as shown in Figures 6(c, d) and it is directed to θ values more than 90° for negative η_z values as shown in Figure 6(e). The vertical radiation patterns for η_z=0, 0.25, 0.5, 0.75, -0.5, -0.25 are shown in Figures 7(a-f), respectively. As mentioned before, the vertical radiation pattern of the rectangular array in Figure 4(a) was not effected by η_z. However unlike the rectangular array, the triangular array in Figure 6a has a vertical radiation pattern which varies with η_z. It can be easily concluded from the figures that the vertical radiation pattern depends on the absolute value of η_z since η_z=0.5 and $\eta_z = -0.5$ produce the same pattern as in Figures 7(c) and (e). The same property can be observed from Figures 7(d) and (f) where the same vertical radiation patterns is obtained for η_z=0.75 and $\eta_z = -0.75$.

Figure 8(a) shows a triangular array consisting of 11 rows (m=0...10) along the x-direction, each with (41-4m) elements along z-direction with its mirror array. The interelement spacings are $d_z = d_x = \lambda/4$ and the normalized interelement phasings are η_z=0.25, η_x=1. While the vertical radiation pattern is shown in Figure 8(b), the horizontal radiation pattern is presented in Figure 8(c). As expected, using more dipoles causes the beam to be narrower.

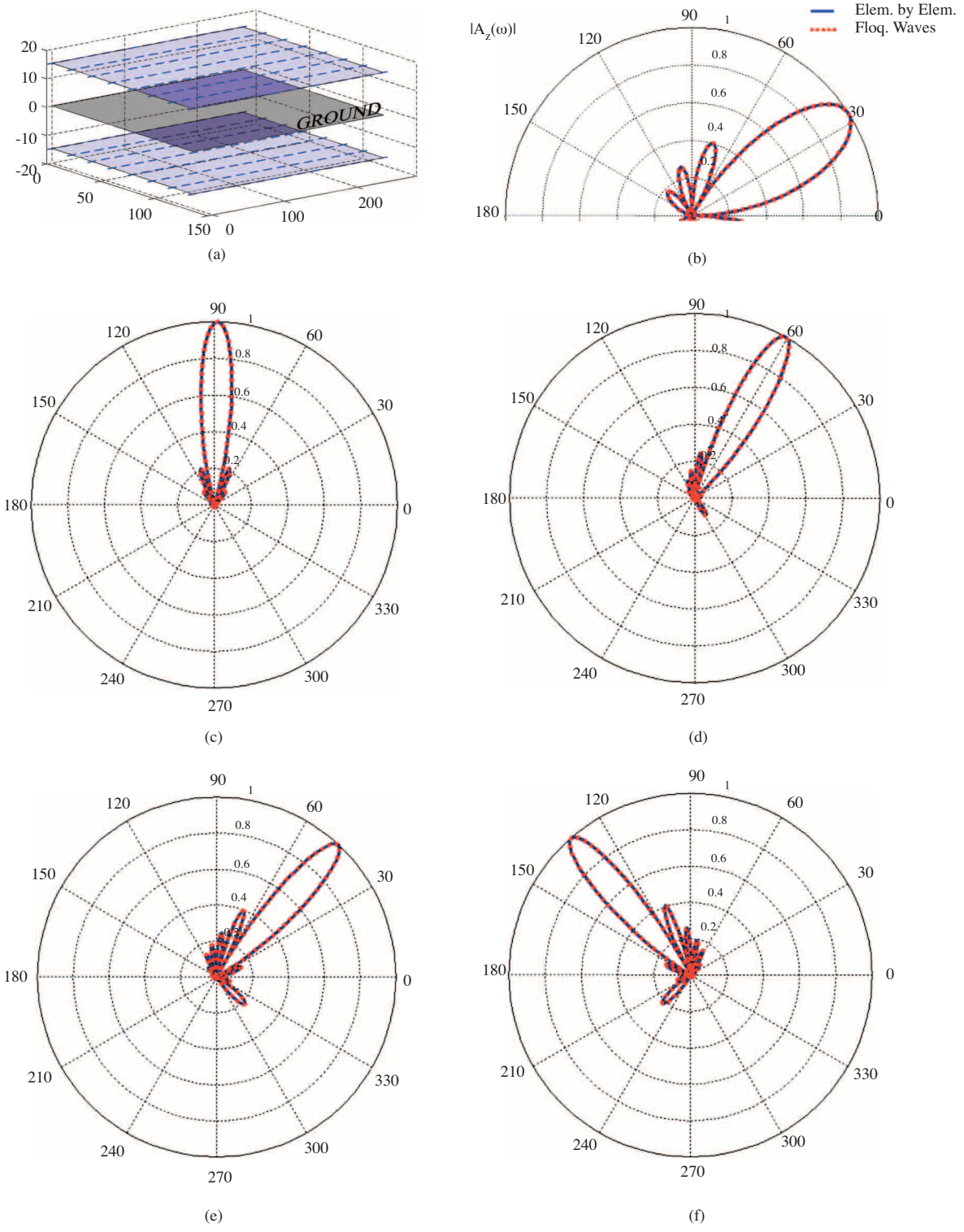

Figure 4. **(a)** Linearly phased, periodic, rectangular array of dipoles and its image array substituting the ground (N_z=15, N_x=8, $d_z = d_x = \lambda/4$, η_x=1) **(b)** Vertical radiation pattern, Horizontal radiation patterns for **(c)** η_z=0, **(d)** η_z=0.5, **(e)** η_z=0.75, **(f)** $\eta_z = -0.75$.

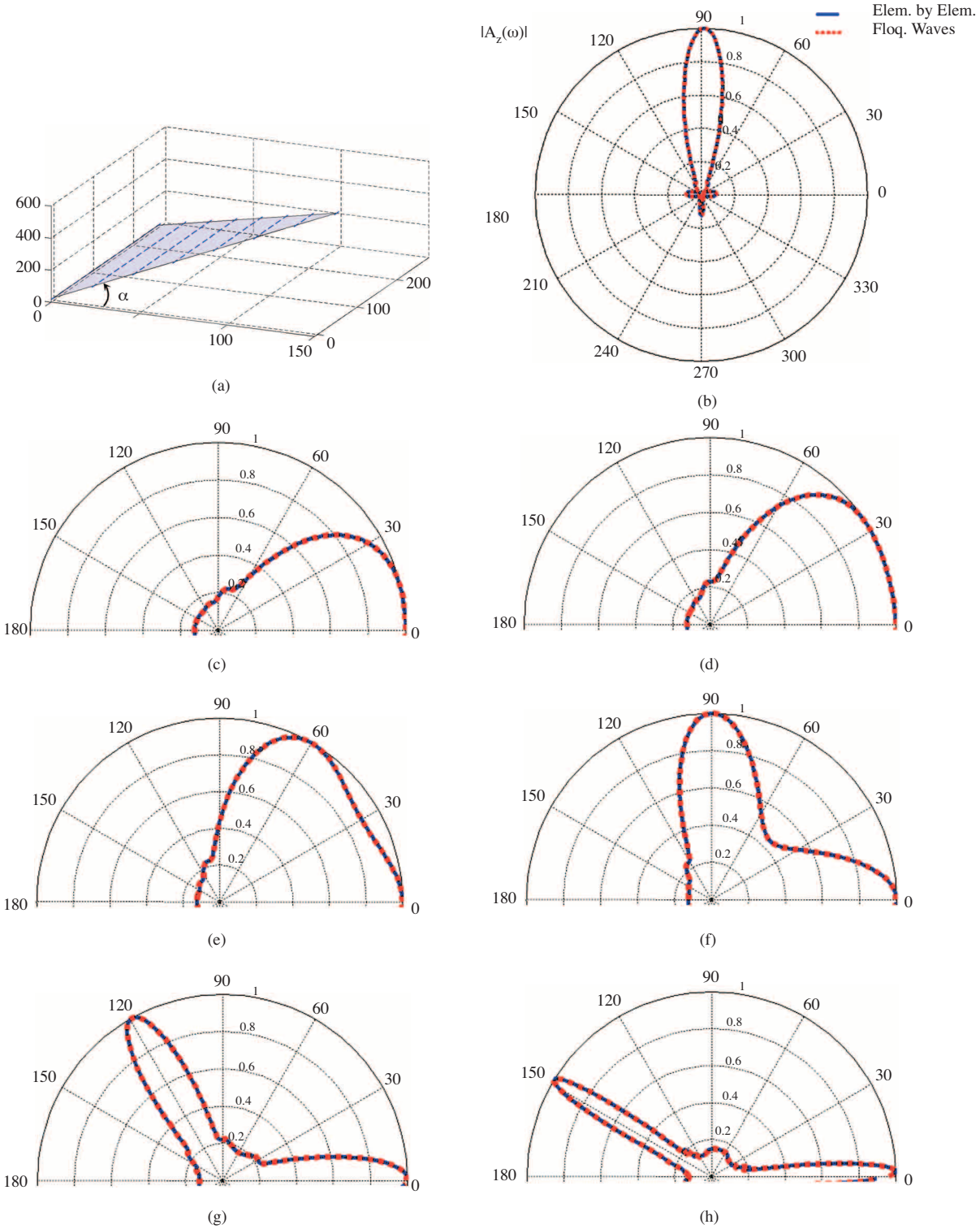

Figure 5. **(a)** Linearly phased, periodic, triangular array of dipoles tilted in the φ direction at an α take off angle (N_z=15-2m, m=0, 1, 2, 3, 4, 5, 6, 7, N_x=8, d_z=d_x = $\lambda/4$, η_z=0, η_x=1) **(b)** Horizontal radiation pattern; Vertical radiation patterns for **(c)** α=0°, **(d)** α=15°, **(e)** α=30°, **(f)** α=45°, **(g)** α=60°, **(h)** α=75°.

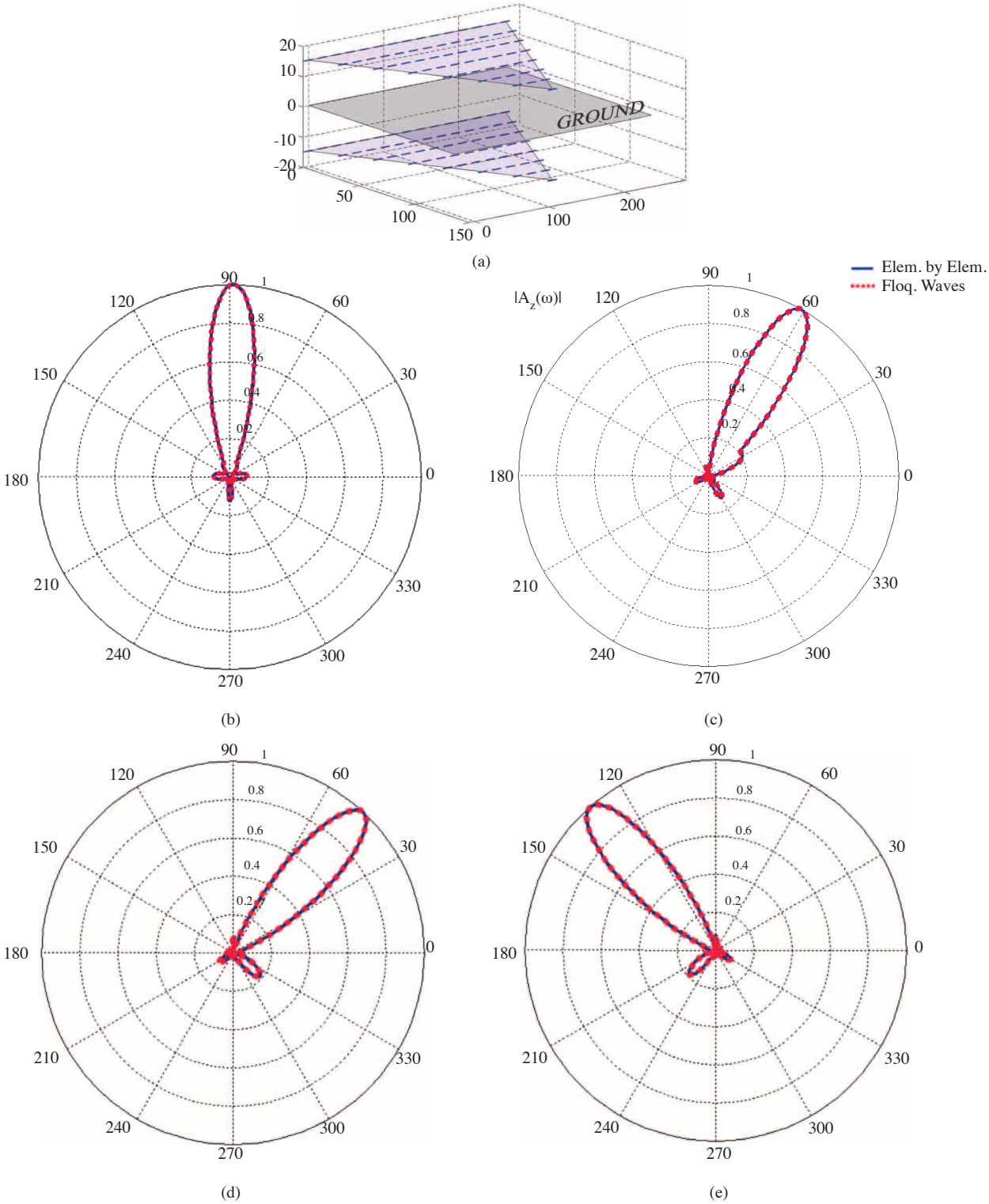

Figure 6. **(a)** Linearly phased, periodic, triangular array of dipoles and its image array substituting the ground (N_z=15-2m, m=0, 1, 2, 3, 4, 5, 6, 7, N_x=8, $d_z = d_x = \lambda/4$, η_x=1, α=0°) Horizontal radiation patterns for **(b)** η_z=0, **(c)** η_z=0.5, **(d)** η_z=0.75, **(e)** $\eta_z = -0.75$.

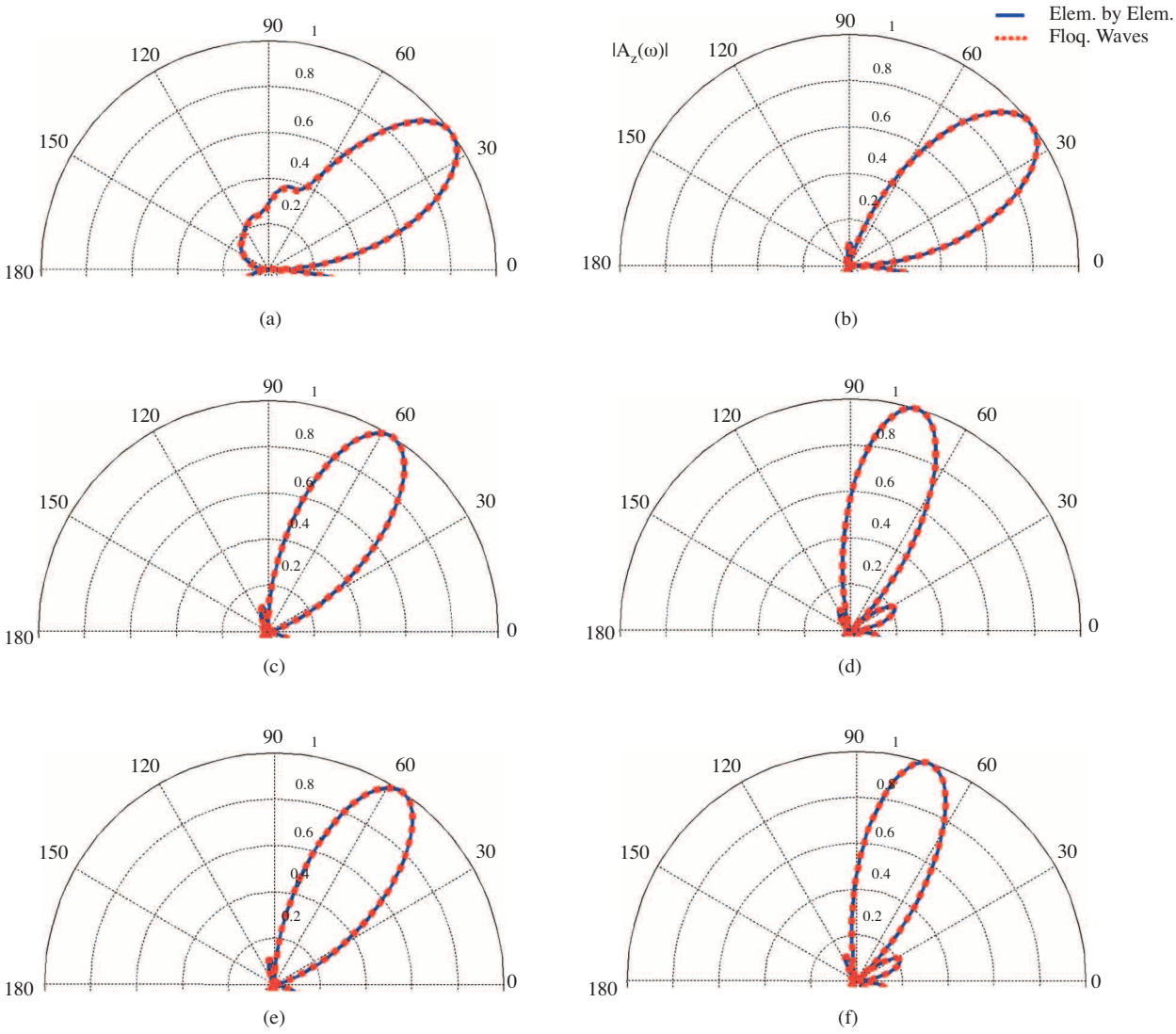

Figure 7. Vertical radiation patterns of the array shown in Figure 6a for **(a)** η_z=0, **(b)** η_z=0.25, **(c)** η_z=0.5, **(d)** η_z=0.75, **(e)** $\eta_z = -0.5$, **(f)** $\eta_z = -0.75$ (d_z=$d_x = \lambda/4$, η_x=1, α=0°).

Figure 8(d) shows a trapezoidal array consisting of 5 rows (m=0,1,2,3,4) along x-direction each with (51-8m) dipoles along z-direction. The interelement spacings are d_z=$d_x = \lambda/4$ and the normalized interelement phasings are η_z=0, η_x=1. Figure 8(e) and 8(f) show the vertical and horizontal radiation patterns, respectively. The horizontal radiation pattern is in the broadside direction with a very narrow beam.

The radiation patterns at the preceding examples were obtained by plotting the amplitude of the magnetic scalar potential $A_z(\omega)$. The electric field can be determined by the z-component of the magnetic vector potential $\vec{A}$ as $E_z = -j\omega\mu A_z + (1/j\omega\varepsilon)\,\partial^2 A_z/\partial z^2$. If the magnetic scalar potential $A_z(\omega)$ is used as defined in (2), the electric field radiated by a triangular array shown Figure 2b can be expressed as

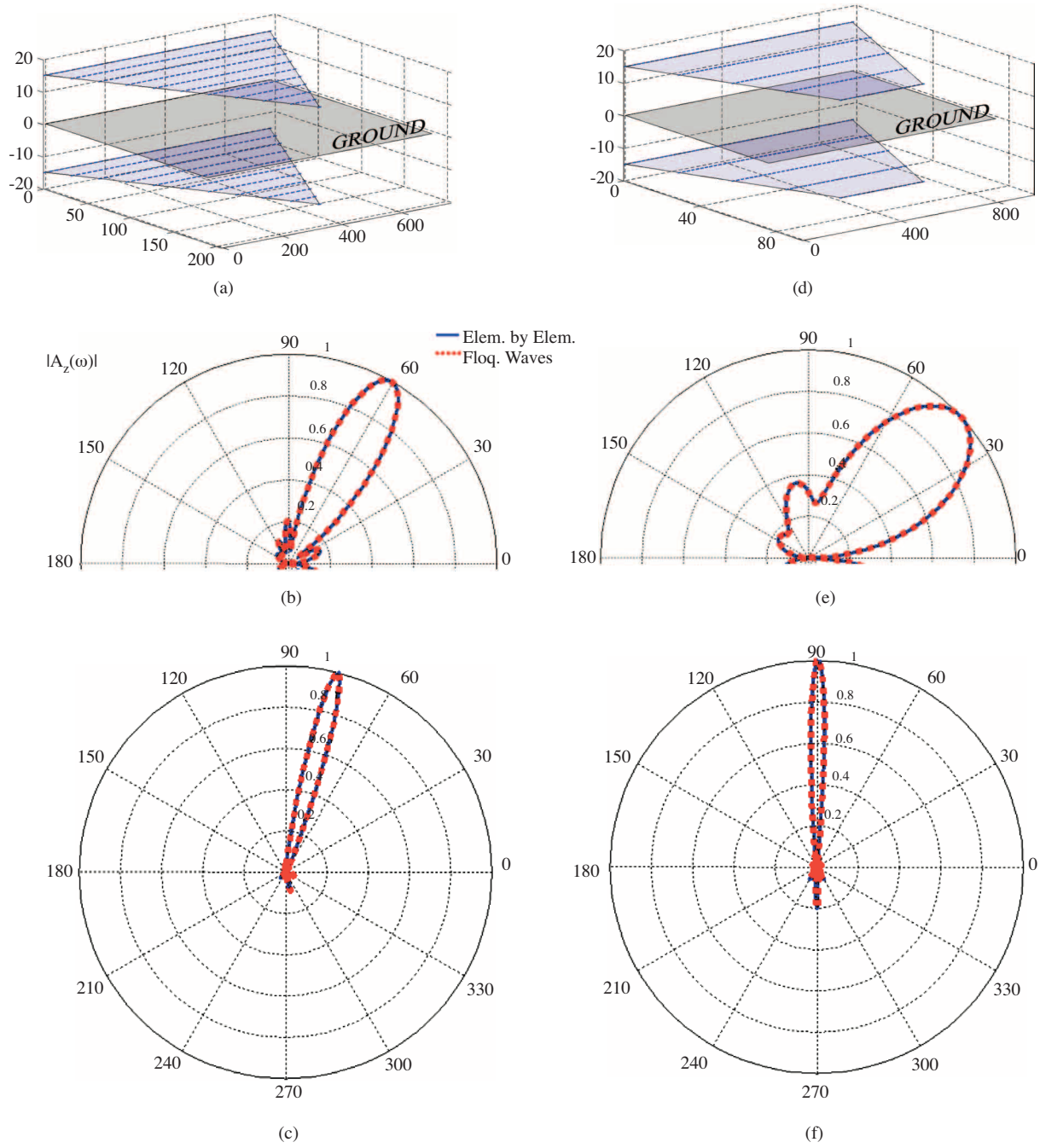

Figure 8. **(a)** Linearly phased, periodic, triangular array of dipoles and its image array substituting the ground (N_z=41-4m, m=0, 1, 2, 3, 4, 5, 6, 7, 8, 9, 10, N_x=11, d_z=d_x = $\lambda/4$, η_z=0.25 η_x=1, α=0°) **(b)** Vertical- **(c)** Horizontal radiation pattern of the triangular array **(d)** Linearly phased, periodic, trapezoidal array of dipoles and its image array substituting the ground (N_z=51-8m, m=0, 1, 2, 3, 4, N_x=5, d_z=d_x = $\lambda/4$, η_z=0 η_x=1, α=0°) **(e)** Vertical- **(f)** Horizontal radiation pattern of the trapezoidal array.

$$E_z(\omega) = \sum_{m=0}^{N_x-1} \sum_{n=m}^{(N_z-1-m)} \frac{30k^2 e^{-jkR_{nm}} e^{-j(k\eta_x m d_x + k\eta_z n d_z)}}{j} \times \left[\frac{1}{kR_{nm}} - \frac{j}{k^2R_{nm}^2} - \frac{1}{k^3R_{nm}^3} + (z-nd)^2k^2\left(\frac{-1}{k^3R_{nm}^3} + \frac{3j}{k^4R_{nm}^4} + \frac{3}{k^5R_{nm}^5}\right)\right] . \quad (4)$$

Figure 9(a) shows the variation of $|E_z(\omega)|$ versus φ in the x-y plane radiated by the triangular array shown in Figure 6a. The array is located over an imperfect ground with the relative permittivity ε_r=15 and the conductivity σ=0.01 S/m. The imperfect ground is modeled by multiplication of the field radiated by the image array with a reflection coefficient defined as

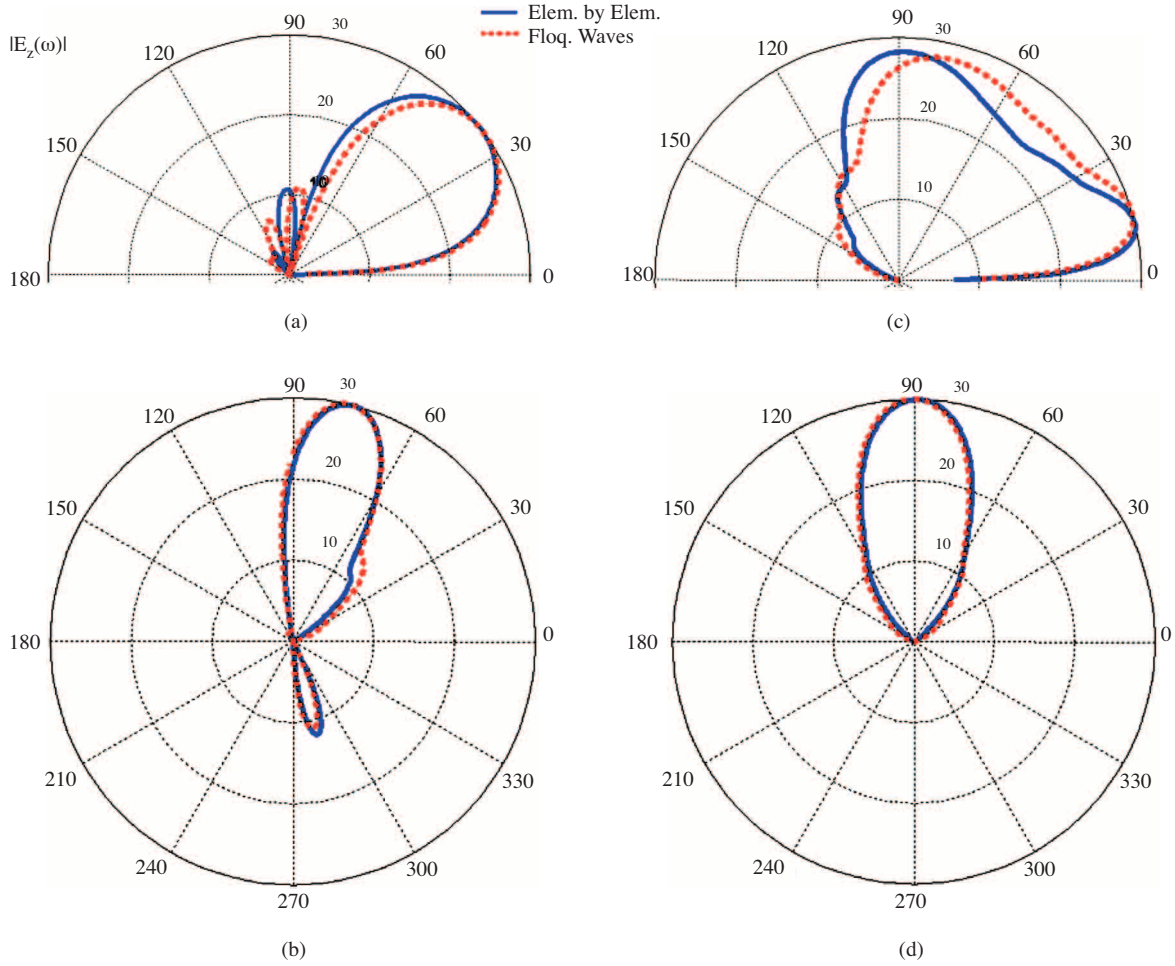

Figure 9. **(a)** Vertical **(b)** Horizontal radiation patterns of the array shown in Figure 6a over an imperfect ground with ε_r=15 and σ=0.01 (N_z=15-2m, m=0, 1, 2, 3, 4, 5, 6, 7, N_x=8, d_z=d_x = $\lambda/4$, η_x=1, η_z=0.25, α=0°) **(c)** Vertical **(d)** Horizontal radiation patterns of the array shown in Figure 5a over an imperfect ground with ε_r=15 and σ=0.01 (N_z=15-2m, m=0, 1, 2, 3, 4, 5, 6, 7, N_x=8, d_z=d_x = $\lambda/4$, η_x=1, η_z=0, α=45°).

$$\rho = \frac{\cos\beta - \sqrt{n^2 - \sin^2(\beta)}}{\cos\beta + \sqrt{n^2 - \sin^2(\beta)}} \tag{5}$$

where $n^2 = \varepsilon_r - j60\sigma\,\lambda$ and $\beta = -\varphi + 90^\circ$. The blue solid curves correspond to element-by-element summation solutions and the red dashed curves correspond to outputs obtained by the software NEC which is based on Method of Moments. Figure 9b shows the horizontal radiation pattern of the same triangular array over imperfect ground with the same relative permittivity ε_r=15 and the same conductivity σ=0.01. Figure 9c shows the vertical radiation pattern of the same triangular array but tilted by a take-off angle α=45° in the φ-direction. The effects of the imperfect ground with ε_r=15 and σ=0.01 are taken into account in the same manner by multiplication of the field radiated by the image array with the reflection coefficient defined in (5). Finally, Figure 9(d) shows the horizontal radiation pattern of the tilted array. While tilting the triangular array by a take-off angle α causes a small change in the horizontal radiation pattern, the vertical radiation pattern totally changes and a new beam appears at 2α. Figures 9(a-d) are plotted in dB scale and they are normalized to 30dBs. It can be observed that the element by element summation solutions agree very well with the NEC solutions. Therefore we can conclude that the effects of imperfect ground are correctly modeled.

4. Conclusion

Skywave HF radar antenna systems are investigated. Different triangular, trapezoidal and rectangular, phased arrays of dipoles are proposed. Beam forming is achieved by using different number of dipoles in different geometrical configurations. The beams are steered by tilting the array by a take-off angle α and also by changing the interelement phasings. Ground effects are also taken into account. Fields are obtained using Floquet wave and element-by-element summation representations, and it's observed that both representations agree very well with each other within the accuracy of the plots.

Acknowledgement

The author would like to thank Leopold B. Felsen Fund for an Award for Excellence in Electrodynamics granted in 2007.

References

[1] L. Sevgi, "Target reflectivity and RCS interaction in integrated maritime surveillance systems based on surface wave HF Radars", *IEEE Antennas and Propag. Magazine*, vol. 43, no. 1, pp. 36-51, Feb. 2001

[2] L. Sevgi, A.M. Ponsford, H.C. Chan, "An integrated maritime surveillance system based on surface wave HF radars, Part I: Theoretical background and numerical simulations", *IEEE Antennas and Propag. Magazine*, vol. 43, no. 4, pp. 28-43, Aug. 2001

[3] A. M. Ponsford, L. Sevgi, H.C. Chan, "An integrated maritime surveillance system based on surface wave HF radars, Part II: Operational status and system performance", *IEEE Antennas and Propag. Magazine*, vol. 43., no. 5, pp. 52-63, Oct. 2001

[4] L. Sevgi, "HF Wire Antenna Array Design via FDTD and MoM Techniques", 1999 IEEE Canadian Conference on Electrical and Computer Engineering, Alberta, Canada, May 9-12, 1999.

[5] L. Sevgi, *Complex Electromagnetic Problems and Numerical Simulation Approaches*, IEEE Press – John Wiley & Sons, Piscataway, New Jersey, 2003.

[6] A. Ishimaru, R. J. Coe, G. E. Miller, and W. P. Geren, "Finite periodic structure approach to large scanning array problems," *IEEE Trans. Antennas Propag.*, vol. 33, no. 11, pp. 1213–1220, Nov. 1985.

[7] L. Sevgi, "Numerical Simulation Approaches for Phased Array Design", *ACES Journal of Applied Computational Electromagnetic Society, Special issue on Phased Array Design*, (invited tutorial), vol. 21, no. 3, pp. 206-217, Nov. 2006.

[8] L. B. Felsen and F. Capolino, "Time domain Green's function for an infinite sequentially excited periodic line array of dipoles," *IEEE Trans. Antennas Propag.*, vol. 48, no. 6, pp. 921–931, June 2000.

[9] F. Capolino and L. B. Felsen, "Frequency- and time-domain Green's functions for a phased semi-infinite periodic line array of dipoles," *IEEE Trans. Antennas Propag.*, vol. 50, no. 1, pp. 31–41, Jan. 2002.

[10] Ç. Uluışık, E. Topuz, L. Sevgi, "Time-domain investigations of periodic rectangular dipole arrays," Workshop on Computational Electromagnetics in Time-Domain (CEM-TD 2007), Perugia, Italy, Oct. 15-17, 2007.

[11] Ç. Uluışık, E. Topuz, L. Sevgi, "Some characteristics of radiation from linearly phased / sequentially excited periodic, rectangular arrays of dipoles," *IEEE Trans. Antennas and Propag.* vol. 56, no. 6, pp. 1794-1798, June 2008.

[12] L. Sevgi, Ç. Uluışık, "A MatLab-based visualisation package for planar arrays of isotropic radiators", *IEEE Antennas and Propag. Magazine*, vol. 47, no. 1, pp. 156-163, Feb. 2005.